PHYSICAL REVIEW D VOLUME 25, NUMBER 7 1 APRIL 1982

Analysis of proton-nucleus and helium-nucleus collisions at energies greater than 10 TeV

S. Tasaka
Institute for Cosmic Ray Research, University of Tokyo, Tokyo, Japan

V. D. Hopper
School of Physics (Royal Australian Air Force Academy), University of Melbourne, Melbourne, Australia

H. Fuchi, K. Hoshino, S. Kuramata, K. Niu, K. Niwa, H. Shibuya, and Y. Yanagisawa
Department of Physics, Nagoya University, Nagoya, Japan

Y. Maeda and H. Kimura
Faculty of Education, Yokohama National University, Yokohama, Japan

Y. K. Lim
Department of Physics, University of Singapore, Singapore

N. Ushida
Faculty of Education, Aichi University of Education, Kariya, Japan

Y. Sato
Faculty of Education, Utsunomiya University, Utsunomiya, Japan
(Received 6 October 1981)

We have studied the characteristics of inclusive γ-ray and charged-meson production in proton-lucite collisions at 20 TeV, and helium-lucite collisions at 7 TeV per nucleon. Characteristics of multiple-production phenomena in these energy regions were fully analyzed and compared with those observed in lower-energy regions. The main results are as follows. (1) A substantial increase of charged secondaries in proton-lucite collisions is observed in the central region as the primary energy increases from 400 GeV to 19 TeV. (2) The average multiplicity in helium-lucite collisions is nearly twice as large as that in proton-lucite collisions at the same energy per nucleon. (3) While no difference is observed of the average values of P_T and P_T^2 for $P_T < 1.0$ GeV/c throughout the energy range studied, the cross section for high-P_T particles ($P_T > 1.0$ GeV/c) substantially increases above 10 TeV. (4) The fractional-energy distribution of γ rays in the range of $0.1 < E_\gamma / \sum E_\gamma < 0.7$ is represented by a single exponential. (5) The scaling of invariant distributions $F_1(x,s)$ for γ rays and charged π mesons in proton collisions at around 10 TeV does not hold in the central region of $x < 0.1$, but the violation of scaling is small in the fragmentation region of $x > 0.1$.

I. INTRODUCTION

Multiple-production phenomena beyond the 10-TeV energy range are very important for extending our knowledge of processes deep in hadronic substance. It is also of interest to compare nucleon-nucleus and nucleus-nucleus collisions at these superhigh-energy regions.

A series of cosmic-ray experiments have been performed with emulsion chambers by many groups.[1-5] The results on transverse-momentum distribution and fractional-energy distribution of γ rays have been reported. To get more extensive information about the characteristics of superhigh-energy nuclear interactions, balloon flights were carried out under the Australia-Japan Collaboration experiment to expose emulsion chambers to cosmic rays. Our emulsion-chamber technique yields the most detailed information about the properties of nucleon collisions and nucleus collisions

in the 10-TeV energy range because it allows detection and energy estimates of charged secondaries as well as of γ rays. We observed 90 high-energy jet showers produced by protons, helium, and heavier nuclei. This article describes (a) proton-lucite collisions centered at the 20-TeV energy range and (b) helium-lucite collisions around 7 TeV per nucleon.

The results are compared with those of 303- and 400-GeV/c collisions produced in similar emulsion chambers by protons from an accelerator. The results are also compared with other accelerator data: the data from proton-proton collisions in the CERN ISR energy range obtained by Thomé *et al.*[6] and the data from α-α collisions with a center-of-mass momentum of 15.6 GeV per nucleon.[7] Combining these data, this article shows how the various properties of inelastic proton collisions and helium collisions vary with energies from ~ 10 GeV up to ~ 10 TeV range.

II. DESIGN AND EXPOSURE OF THE EMULSION CHAMBER

A. Design of the emulsion chamber

The structure of the small emulsion chambers, as well as the method of scanning and measuring of secondary particles have been described in a review paper.[8] A typical configuration of the emulsion chamber is shown in Fig. 1. The chamber has three sections: upper, middle, and lower. The upper is used to determine the charge of the incident particle. The charge identifier is composed of several sheets of thick emuslion films of 300 μm coated on both surfaces of polystyrene base 150-μm thick. The middle section, consisting of lucite plates interleaved with thin layers of nuclear-emulsion plates, is used not only as a target layer but also to locate each interaction vertex and measure the emission angles of the secondary charged particles. The lower section is used to estimate the energies of secondary charged particles and γ rays. This analyzer layer consists of a sandwich of lead plates, nuclear-emulsion plates, and x-ray films. The x-ray films interleaved in this part are utilized as a detector of jet showers. The overall size of the emulsion chamber is about 20 cm$\times$25 cm$\times$23 cm with a mass of 50 kg. A characteristic feature of these assemblies is that the particles traverse the sandwiches nearly perpendicular to their planes for most accepted events. The thickness of the target layer is 17 cm; this corresponds to 0.26 interaction mean-free paths for nucleons. The thickness of the analyzer layer is 10 radiation lengths.

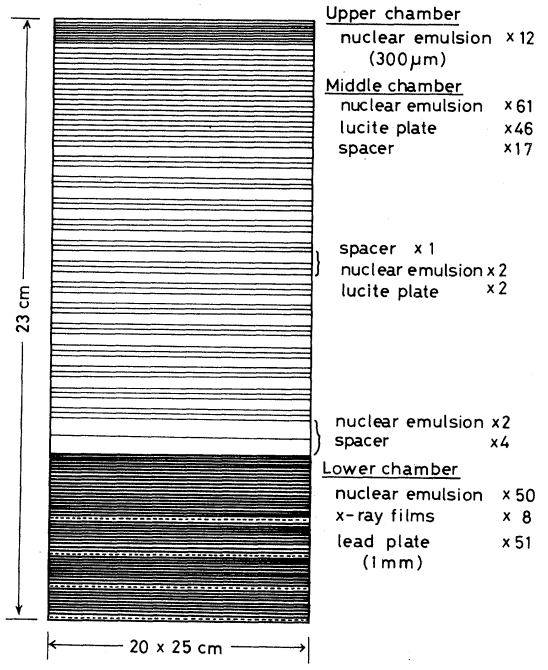

FIG. 1. Configuration of an emulsion chamber.

B. Exposure of the emulsion chamber

The emulsion chambers of this type were exposed to cosmic rays using balloons launched by the Australian Balloon Launching Station at Mildura in 1978 and 1979. The two exposures were made for 32.5 h and 12.0 h at average height of 12 and 20 g/cm^2, respectively. The total exposure amounts to 14 m^{2}h. Effective $S\Omega T$ for nuclear interactions produced by proton and helium with zenith angles less than 45° were estimated to be 1.9×10^4 and 2.5×10^4 m^2 sr sec, respectively, taking account of attenuation in the air and the target design.

III. EXPERIMENTAL METHODS

A. Detection of jet showers

The x-ray films interleaved in the analyzer were scanned by the naked eye for dark spots due to cascade showers induced by γ rays. Cascade showers with energies higher than 400 GeV were detected with sufficient efficiency. The events

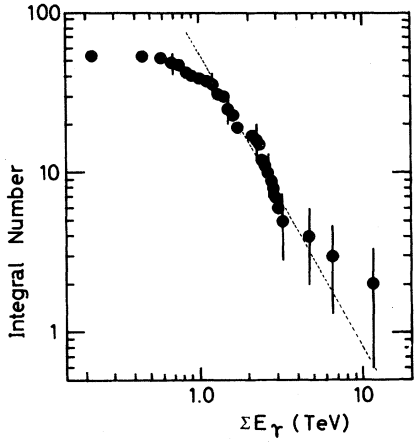

FIG. 2. The integral spectrum of $\sum E_\gamma$, the total energy carried away by γ rays. The dotted line shows the $N(>\sum E_\gamma)=\text{const}\times(\sum E_\gamma)^{-\beta}$ with $\beta=1.7$.

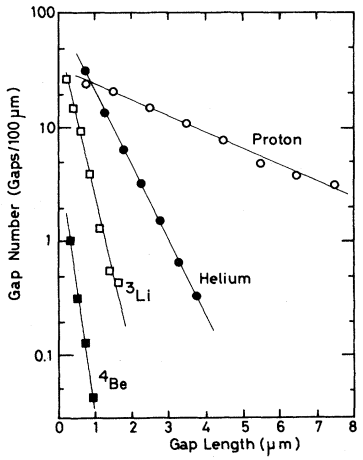

FIG. 3. Gap-length distributions are shown for proton, helium, and light nuclei. The solid lines show the distributions of $N(>L)=\text{const}\times\exp(-\Gamma L)$.

were then traced back using the emulsion plates, and finally the origins of jet showers were detected in the target section. Although the actual interaction vertex is normally in the lucite and not visible, its position can be determined with an accuracy of a few tens of micron. The track of the incident particle can be found, and its charge be determined. The scanning efficiency for nuclear collisions and detection bias were examined by the integral spectrum of the total energy carried away by γ rays, i.e., $\sum E_\gamma$. The integral $\sum E_\gamma$ spectrum in 53 events is shown in Fig. 2, and it can be approximated by a power law in the region of $\sum E_\gamma > 1.2$ TeV:

$$N(>\sum E_\gamma)=\text{const}\times(\sum E_\gamma)^{-\beta}\,, \tag{1}$$

where β is 1.7. The scanning efficiency for nuclear collisions with $\sum E_\gamma > 1.2$ TeV was close to unity.

B. Determination of the charges of incident particles

The method of charge determination for incident particles utilized in this experiment is the same as that applied in the emulsion stack[9]: that is, by gap-length measurement for proton, helium, and light nucleus, and by a method of counting δ rays with four or more grains for heavier nuclei. The number of gaps with length greater than L decreases exponentially:

$$N(>L)=\text{const}\times\exp(-\Gamma L)\,, \tag{2}$$

where Γ gives a measure of mean gap length, as $\langle L\rangle=1/\Gamma$. This Γ value depends on the primary charge Z, as $\Gamma=AZ^2$, where A is a constant. Figure 3 shows the gap-length distributions for proton, helium, and light nucleus. In our experimental condition, we get $A=0.34\pm0.03\ \mu\text{m}^{-1}$ by calibration.

The density of δ rays with four or more grains gives a measure of the charge by the formula

$$N_\delta(\text{per}100\ \mu\text{m})=BZ^2+C\,, \tag{3}$$

where B and C are the constants. In our experimental condition, the choice of $B=0.10$ and $C=-0.04$ gives the best fit for light, medium, and heavy nucleus.

By means of the methods mentioned above, the charges of incident particles of 90 high-energy jet showers were determined: 50 of them were produced by protons, 23 by helium, 10 by light, and 7 by heavier nuclei. Two kinds of target nucleus are involved in these experiments, 82 events occurred in lucite plates ($C_5H_8O_2$), and 8 events in the emulsion (mainly AgBr).

C. Measurement of emission angles

The incident axis of the jet shower is assumed to be the energy-weighted center of γ rays and charged particles, that is, the position of the axis (a,b) in the plane of the detector emulsion was determined from the following expressions:

$$a=\sum(E_i x_i)\Big/\sum E_i\,,\qquad b=\sum(E_i y_i)\Big/\sum E_i\,, \tag{4}$$

where x_i and y_i are the locations of the γ rays and charged secondary particles, and E_i is the energy. The summation was taken over γ rays with energy $E_\gamma > 30$ GeV and all charged secondary particles.

In the case when the momenta of charged particles were not measured, the energy-weighted center of γ rays was first estimated. Next, energy of each charged particle was estimated assuming constant transverse momentum of 0.4 GeV/c relative to it, and then the final energy-weighted center was obtained using formula (4). For the events in which energy of γ rays was not measured, the center of charged particles estimated by assuming constant transverse momentum was regarded as the shower axis. The emission angles θ of all the secondary particles were determined in relation to the axis defined above.

To examine the uncertainty of the above axis determination the angle θ_{axis} between the true incident axis and an energy-weighted axis was estimated by the data of 303- and 400-GeV/c collisions produced by protons from an accelerator.[10] In this case, the relative angle between secondary particles and noninteracting beam tracks can be measured accurately enough. Special care taken in assembling the chamber enabled us, in favorable cases, to measure the relative angle between tracks of charged particles with error less than 10 μrad. The uncertainty of the axis was found to be $(5.5\pm0.7)\times10^{-4}$ and $(3.9\pm0.7)\times10^{-4}$ rad in 303- and 400-GeV/c collisions, respectively. Figure 4 shows the distribution of the θ_{axis} estimated from 70 collisions in 303-GeV/c protons. The area with 250-μm radius was scanned under a microscope to detect the secondary charged particles in the nearest emulsion plate downstream of the collision vertex. We can find the charged particles emitted within 0.2 rad from the axis. The emulsion area within 10 mrad in the lower chamber was scanned to detect the secondary γ rays.

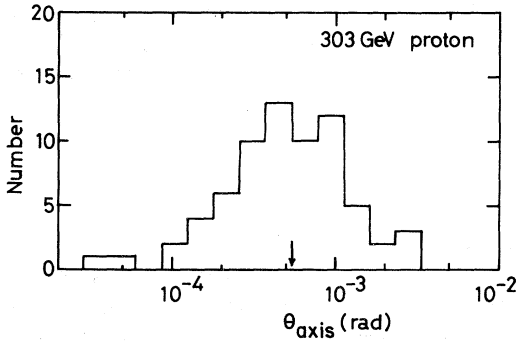

FIG. 4. The distribution of θ_{axis}, the angle between an incident axis and an energy-weighted center which was estimated by the data of 303-GeV proton collisions from accelerator.

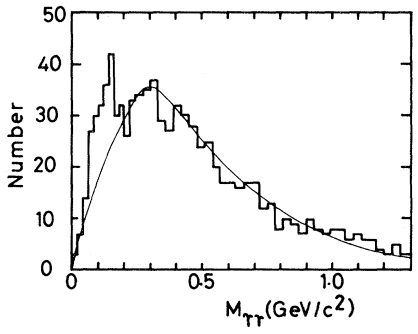

FIG. 5. Distribution of invariant mass $M_{\gamma\gamma}$ of pair of γ rays with $E_\gamma > 30$ GeV and $\theta_\gamma < 10^{-2}$ rad. The solid curve shows the background which was calculated by the Monte Carlo program.

D. Energy and momentum measurement of γ rays and charged particles

Cascade showers induced by tertiary γ rays from neutral pions are followed toward the downstream end of the chamber. The number of shower electrons in the circle with radius of 25 or 50 μm was measured at various depths. The energy of a γ ray is estimated by fitting counted data to the curves derived from the three-dimensional cascade-shower theory taking into account the effect of the spacing between main scattering substances.[11] The calibration of this method was made by two independent methods. One was by finding the π^0-meson peak in the invariant-mass distribution of any two γ rays in the same event. Figure 5 shows the invariant-mass distribution of γ-ray pairs of all events. A clear peak was observed at $M_{\gamma\gamma}=135$ MeV/c^2 and clearly distinguished from the background. The energy resolution for γ rays was estimated to be 20% by the width of this peak. Another was by carrying out the exposure of the similar type of emulsion chamber to electron beams of 50 and 300 GeV at Fermilab.[8,10,12] The agreement of observed data with the theoretical curves is quite satisfactory.

For charged particles, the relative scattering method is applied to estimate their momentum. High precision in measurement of the relative distances between secondary tracks, and high scatter-

TABLE I. Events in which $\sum E_\gamma$ has been measured.

Event name	n_γ	n_s	$\sum E_\gamma$ (GeV)	$\sum E_{ch}$ (GeV)	E (GeV/nucleon)
Proton-lucite					
B7E001	5	10	1438	4171	9347
B7E017	9	17	1187	3325	7520
B7E022	3	13	2557	5914	14 118
B7E031	16	58	1285	12 040	22 208
B7E064	6	3	853	553	2344
B7E088	2	19	629	2892	5868
B7E097	7	11	1018	957	3292
B7E146	5	22	505	1577	3469
B8E004	3	21	1170	695	3109
B8E041	9	16	1945	5641	12 644
B8E084	16	20	5484	2812	13 825
B8E098	7	15	1450	3254	7839
B8E119	16	48	3910	5730	16 066
B7F007	6	11	1171	2246	5696
B7B001	6	15	2310	4051	10 602
B7B015	7	30	1600	1498	5164
B7B028	2	8	1200	439	2732
B7B029	7	12	1670	6464	13 557
B7B014	2	7	2200	335	4225
B8D003	5	39	2800	3681	10 802
B7D011	5	18	670	2178	4747
B7D037	8	11	790	593	2304
B7D076	3	26	740	3352	6819
B7D098	5	15	570	1487	3429
B7D104	4	3	850	496	2243
B8C002	4	6	1550	217	2944
B8C006	7	17	3200	2327	9212
B8C018	11	42	1010	1243	3755
Proton-emulsion					
B8E030	16	86	1963	2190	6922
B8A001	8	71	2204	8828	18 386
B7B003	9	32	2160	1615	6291
B7D017	7	47	870	3111	6635
Helium-lucite					
B7E061	16	42	2315	3949	5220
B8E083	26	52	2132	4044	5147
B7F001	13	65	759	1933	2244
B7F002	15	51	1285	2762	3372
B7F005	24	83	1330	4954	5237
B7B004	7	26	1420	3028	3706
B7B013	6	29	1260	3272	3776
B8D001	18	47	11 430	10 901	18 609
B8D004	7	64	1409	4648	5048
B8D014	2	25	570	690	1049
B7D059	4	$14+\alpha$	220	686	755
B7C016	11	16	777	1738	2096
Helium-emulsion					
B7E077	58	186	9711	26 816	30 439

ing signal due to lead nuclei allow us to estimate momentum up to the TeV/c region.[8,10] The relative scattering method was calibrated by exposing a similar type of emulsion chamber to proton and negative pion beams from 10 to 400 GeV/c at Fermilab and ANL.

E. Estimation of primary energy

The primary energy of observed jet showers was estimated by using the equation

$$E \text{ (per nucleon)} = \sum E_\pi / K_p / \langle \nu \rangle \tag{5}$$

with

$$\langle \nu \rangle = A_B(\sigma_{pT}/\sigma_{BT})$$

and

$$\sum E_\pi = \sum E_\gamma + \sum E_{\text{ch}} ,$$

where we assumed that an incident nucleus with a mass number A_B and the energy E per nucleon collides with a target nucleus of a mass number A_T (this value was assumed to be 11 for the lucite target). The value of K_p is the mean inelasticity coefficient for proton-nucleon collisions, which is assumed to be 0.6.[13] The value of $\langle \nu \rangle$ can be taken as the average number of interacting nucleons for a given incident nucleus, and σ_{pT} and σ_{BT} are inelastic proton-nucleus cross section and nucleus-nucleus cross section. σ_{BT} is given by the expression

$$\sigma_{BT} = r_0^2[A_B^{1/3} + A_T^{1/3} - b_0(A_B^{-1/3} + A_T^{-1/3})]^2 , \tag{6}$$

where $r_0 = 1.36$ fm and $b_0 = 0.75$.[14] The value of $\langle \nu \rangle$ is calculated to be 2.0 for helium in the lucite target. The value of $\sum E_\gamma$ and $\sum E_{\text{ch}}$ are the sums of the energy carried away by neutral and charged mesons, respectively. The values $\sum E_\gamma$ were measured for 45 events listed in Table I. In most cases, $\sum E_{\text{ch}}$ is estimated by

$$\sum E_{\text{ch}} = \sum (0.4 \csc\theta_{\text{ch}}) \text{ GeV} ,$$

assuming constant P_T of 0.4 GeV/c. The proton and/or other fragments emitted in the most forward direction should be excluded from the charged secondaries in this formula.

The above equation was checked by applying it to the jet showers produced by accelerator protons with energy of 303 and 400 GeV/c. The primary energies thus estimated turned out to be 288 ± 15 and 450 ± 30 GeV for 303 and 400 GeV/c, respectively. Figure 6 shows the distribution of primary energy estimated from 70 proton collisions at 303 GeV/c. The dispersion of the estimated primary energy in Figure 6 is 125 GeV/c; that is about 40%. The average value of $\sum E_{\text{ch}} / \sum E_\gamma$ was evaluated to be 1.8 in 32 proton events, and 2.0 in the other 21 nucleus events in which $\sum E_\gamma$ was measured. These values were used in estimating primary energy for another 38 events for which $\sum E_\gamma$ was not measured, and the results are listed in Table II for proton and helium.

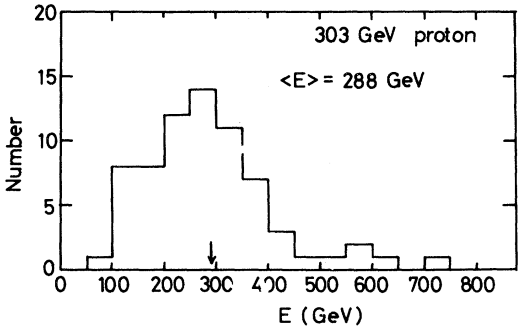

FIG. 6. The distribution of primary energy E estimated by Eq. (5) for 303-GeV proton collisions.

The mean incident energy of primary particles was estimated to be $\langle E_p \rangle = 19 \pm 4$ TeV in 21 protons with energies over 7 TeV, and $\langle E_\alpha \rangle = 9 \pm 3$ TeV per nucleon in 11 helium nuclei with energies over 3.5 TeV per nucleon. These events are free from detection bias, as described below in the primary energy spectra.

IV. EXPERIMENTAL RESULTS

A. Primary energy spectra

The integral primary energy spectra for proton and helium are shown in Fig. 7. The detection of events is free from bias for proton with energy greater than 7 TeV, and for helium with energy greater than 3.5 TeV per nucleon. In estimating the absolute intensities of the primary proton and helium, corrections due to the effective aperture of the detector and due to the absorption in the upper atmosphere were taken into accounnt. A Monte Carlo study was carried out to estimate the absorption effect of the atmosphere with collision mean-free path of 80 and 48 g/cm^2 for proton and heli-

TABLE II. Events in which $\sum E_\gamma$ has not been measured.

Event name	n_s	$\sum E_{ch}$ (GeV)	E (GeV/nucleon)
Proton-lucite			
B7A003	12	5775	14914
B7A022	32	11425	29503
B7A026	33	41635	107520
B7A052	16	1784	4606
B7A075	18	2612	6745
B7A072	31	6875	17753
B7B024	30	7316	18892
B7C002	13	1113	2874
B7C008	33	2878	7432
B7C015	24	1914	4944
B7C064	36	4754	12277
B8B002	20	449	1161
B8E024	4	509	1315
B8E031	16	3504	9048
B8E065	36	1501	3876
B8E078	25	1482	3828
B8E107	9	724	1869
Proton-emulsion			
B8B003	33	880	2273
Helium-lucite			
B7A005	27	6508	8135
B7A062	43	1034	1292
B7C037	18	682	852
B7C055	18	273	341
B7D128	32	626	783
B8E044	71	7667	9583
B8E045	11	3000	3750
B8E073	6	217	272
B8E096	40	1692	2115
B8E157	$7+\alpha$	2456	3071

um. The absolute intensities of primary proton and helium thus obtained are

$$I(E>10\ \text{TeV})=(8\pm2)\times10^{-4}\ \text{per m}^2\text{sr sec}$$

and

$$I(E>5\ \text{TeV per nucleon})=(3\pm1)\times10^{-4}\ \text{per m}^2\text{sr sec},$$

respectively. These results are not inconsistent with the extrapolation from low-energy regions obtained by Ryan *et al.*[15]

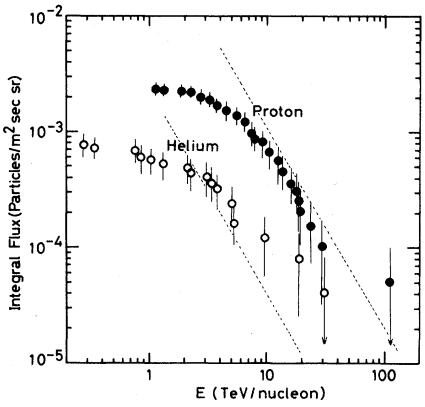

FIG. 7. Integral primary energy spectra for proton and helium. The dotted line shows the extrapolation from low-energy regions obtained by Ryan *et al.*

B. Emission angles and energies of γ rays and charged particles

The data on the emission angles of the secondary charged particles for 50 proton collisions and 23 helium collisions are summarized in Fig. 8. The data on energies and emission angles of γ rays are summarized in Figs. 9 and 10 for 32 proton collisions and 13 helium collisions, respectively. In the following analysis, we restrict ourselves only to the lucite events for simplicity.

C. Multiplicity of the secondary charged particles

There are 45 proton-lucite collisions of which 20 events have incident energy greater than 7 TeV. The average incident energy $\langle E_p \rangle$ is estimated to be 19 ± 4 TeV, which corresponds to a total center-of-mass energy of 200 GeV. The multiplicity distribution of charged secondaries in the high-energy group has a mean multiplicity $\langle n_s \rangle_{pA}=25.2\pm3.0$, with a standard deviation $(\langle n_s^2 \rangle_{pA}-\langle n_s \rangle_{pA}^2)^{1/2}=13.4$. Corrections must be made to compare this value with that for proton-proton collisions. This value must be corrected for (a) bias against detection of charged particles emitted in the backward direction, (b) nuclear-target effect, and (c) bias against events with $\sum E_\gamma<1.2$ TeV. A 9% correction is made for missing charged secondaries in the backward direction (i.e, $\theta_{ch}>0.2$ rad). The nuclear-target effect has been studied in emulsion chambers by Fumuro *et al.*[16] This effect is estimated using the following formula:

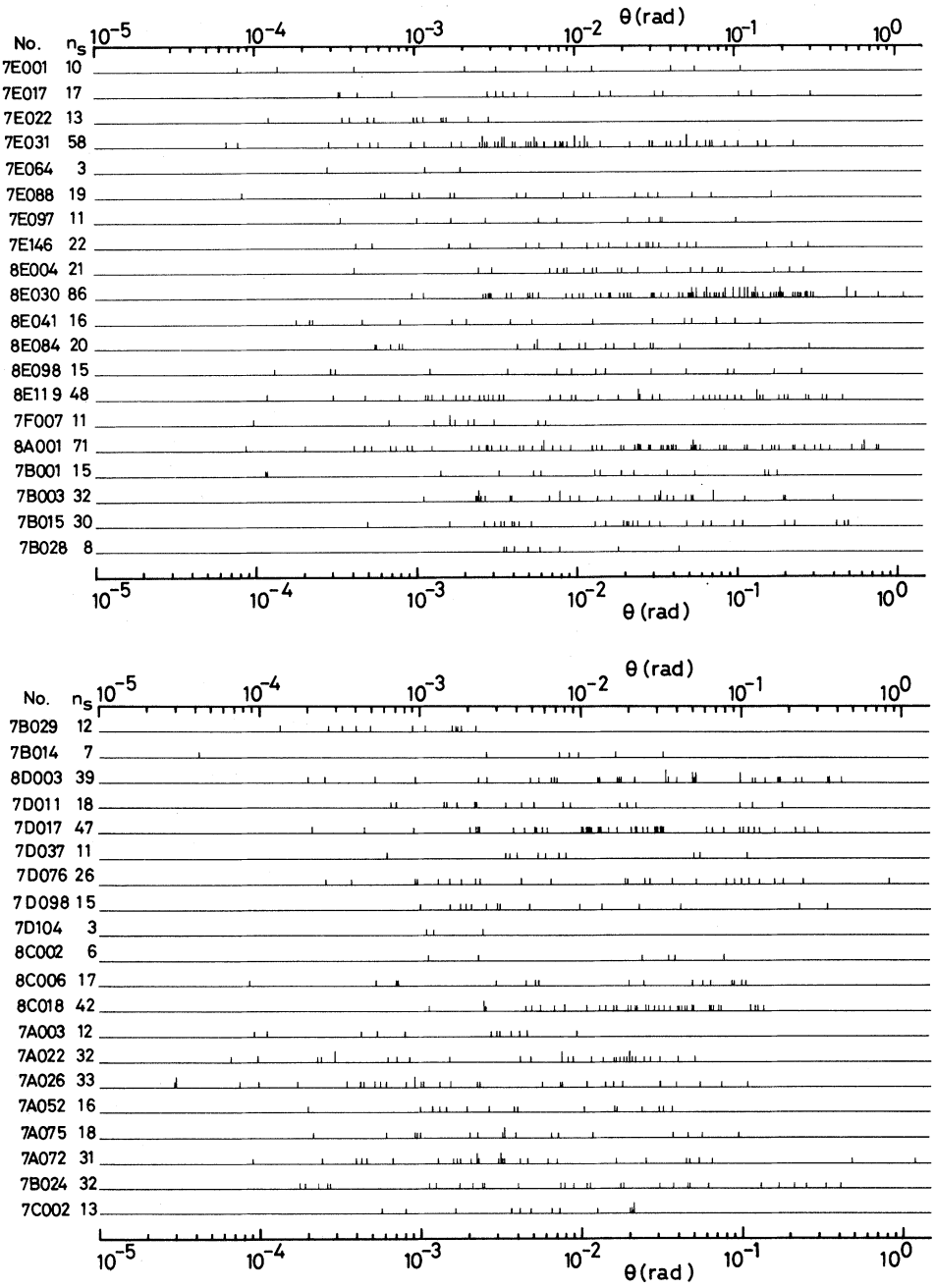

FIG. 8. The data on the emission angles of the secondary charged particles relative to the estimated axis in individual jet shower. The left end of the line lists the event number and multiplicity of charged secondary particles, n_s.

$R_A = \langle n_s \rangle_{pA} / \langle n_s \rangle_{pp} = A^{0.17}$, where $\langle n_s \rangle_{pp}$ and $\langle n_s \rangle_{pA}$ are the average charged multiplicities in proton-proton and proton-nucleus collisions. The value for lucite target is calculated to be $R_A = 1.5$. This value agrees with the experimental result obtained by Jain *et al.*[17] We examined a possible effect of bias for projectile and/or target dissociation processes, since the target dissociation process was missed in our detection. We detected two events B7E064 and B7D104 both with $n_s = 3$, known as projectile dissociation. In these events, all secondary charged particles are emitted with emission

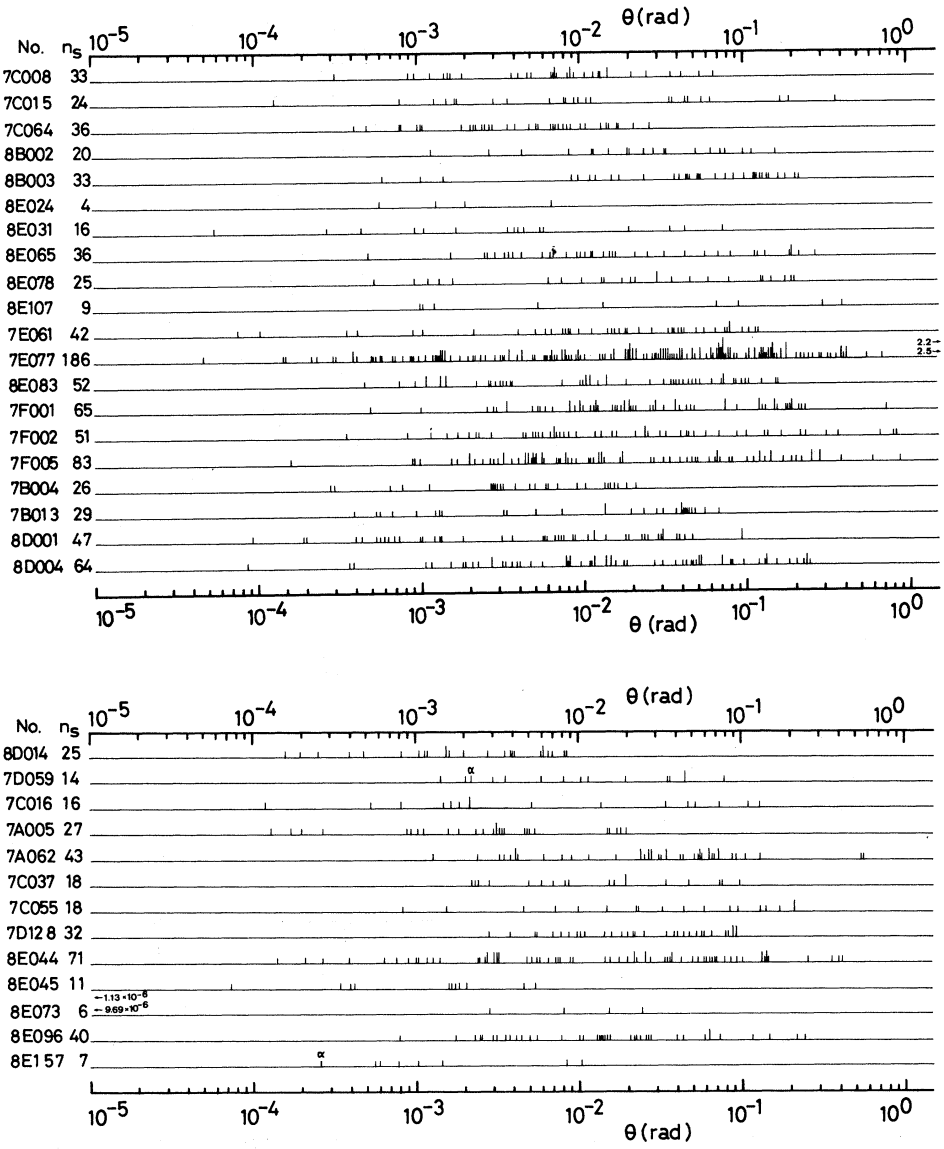

FIG. 8. (*Continued.*)

angles of the order of 1 mrad, and the primary energies are estimated to be about 2 TeV. We are analyzing only events with energies greater than 7 TeV; therefore, we conclude the bias against target dissociation is negligible in obtaining the average multiplicity, assuming forward and backward symmetry of the dissociation. Consequently, the corrected average multiplicity of secondary charged particles in proton-nucleon collisions is $\langle n_s \rangle_{pp} = 18.3 \pm 2.2$ at the mean energy of 19 TeV.

We have exposed a similar type of emulsion chamber to accelerator proton beams for the purpose of calibration. In the emulsion-chamber experiment at 400-GeV proton, we found the mean charged multiplicity $\langle n_s \rangle_{pA} = 13.5 \pm 1.1$ after correction of missing charged particles, and obtained $\langle n_s \rangle_{pp} = 9.0 \pm 0.8$. The mean charged multiplicity in proton-proton collisions at 400 GeV has been shown to be 9 in the bubble-chamber experiment.[18] Since this agrees well with the corrected value found by the emulsion chamber, it is reasonable to take the above procedure of correction also in the cosmic-ray experiment.

There are 22 helium-lucite interactions, of which 10 events have been estimated to have an incident energy greater than 3.5 TeV per nucleon. The

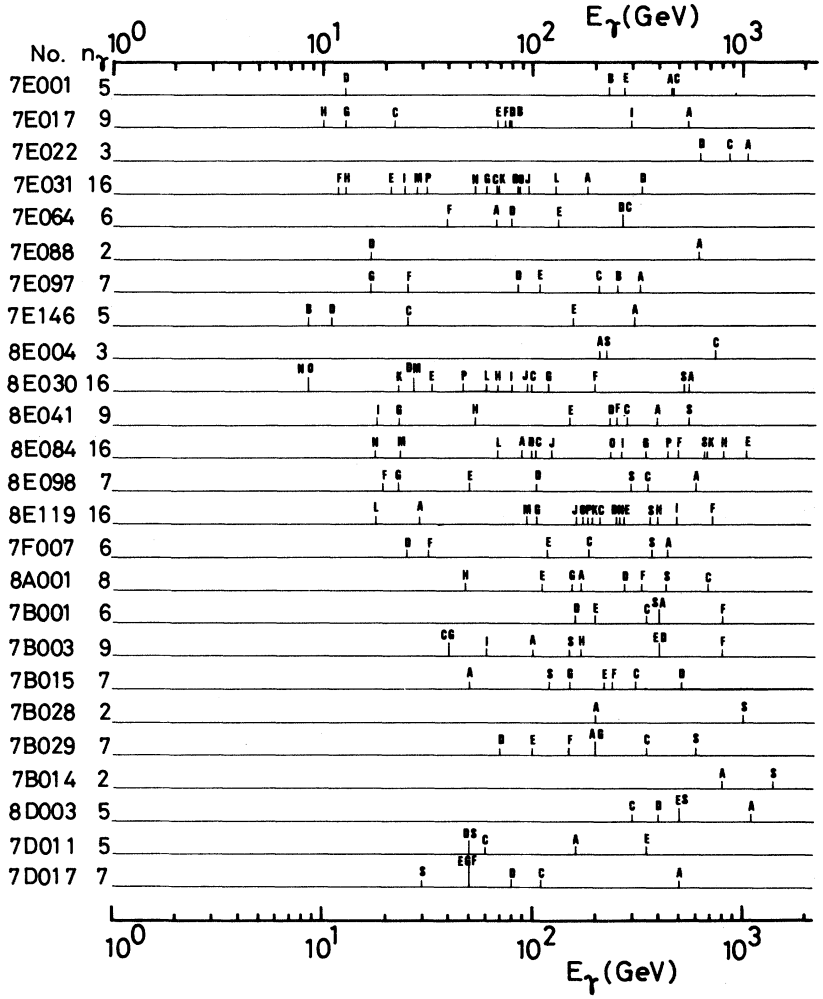

FIG. 9. The data on the energies of γ rays E_γ, in individual event. The left end of the line lists the event number and multiplicity of γ rays, n_γ.

average charged multiplicity of these 10 events was obtained as $\langle n_s \rangle_{\alpha A} = 49.3 \pm 7.8$ after correction for missing charged particles, with the standard deviation $(\langle n_s^2 \rangle_{\alpha A} - \langle n_s \rangle_{\alpha A}^2)^{1/2} = 22.7$. The average incident energy is $\langle E_\alpha \rangle = 7 \pm 2$ TeV per nucleon.

D. Angular distributions of charged particles and γ rays

The angular distribution of secondary particles is defined as follows:

$$\frac{1}{\sigma_{\text{inel}}} \frac{d\sigma}{d\eta^{\text{c.m.}}} = \frac{1}{n} \frac{dN}{d\eta^{\text{lab}}} , \qquad \eta^{\text{c.m.}} = \eta^{\text{lab}} + \tfrac{1}{2} \ln \frac{1-\beta}{1+\beta} , \tag{7}$$

where $\eta = -\ln(\tan\theta/2)$ is the pseudorapidity, β is the relative speed of c.m. to laboratory system, n is the number of observed events, and N is the total number of secondary particles. The angular distribution of charged secondary particles produced in proton-lucite collisions with energy greater than 7 TeV is shown in Fig. 11(a). It should be noticed that some of the most backward-emitted particles are missed by scanning bias. The result in 400-GeV proton collisions is also shown in the same figure after boosting to 20 TeV for comparison. A detector of similar type was used in the 400-GeV accelerator experiment, and the target nuclei were the same.

In order to examine the scaling behavior of the angular distribution of secondary particles, we studied the number density of secondary charged

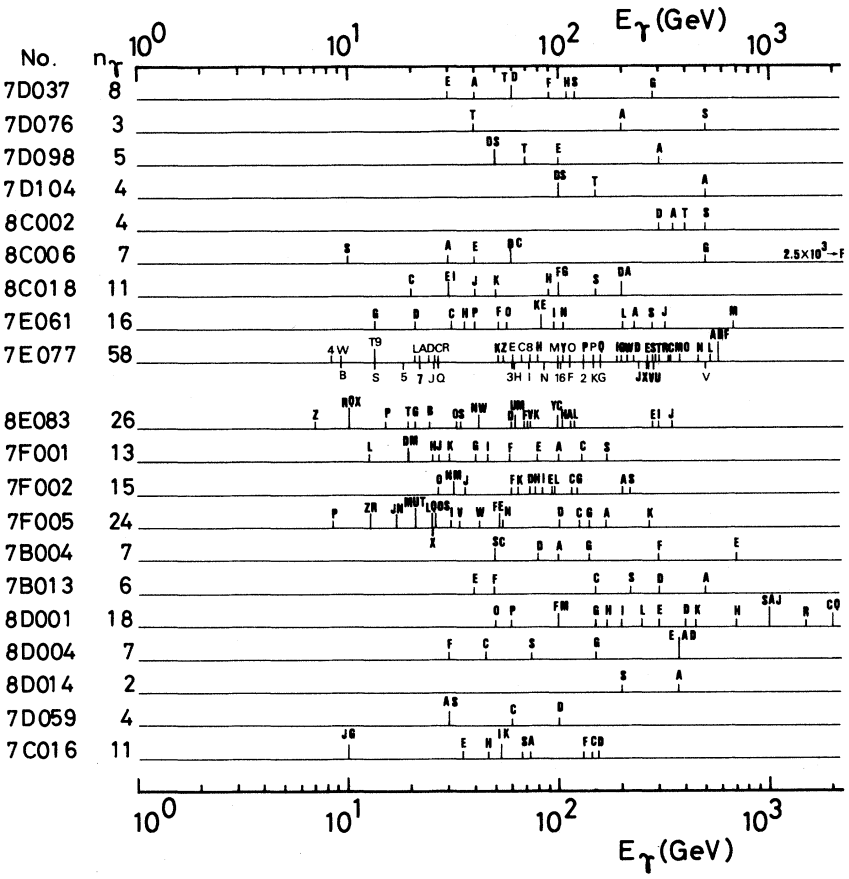

FIG. 9. (*Continued.*)

particles in the central region of $|\eta^{\text{c.m.}}| < 1.5$. This region corresponds to the region of $3.80 < \eta^{\text{lab}} < 6.80$ for proton interactions with incident energy around 20 TeV, and $3.27 < \eta^{\text{lab}} < 6.27$ for helium interactions with incident energy around 7 TeV per nucleon. Average multiplicities of charged particles in $|\eta^{\text{c.m.}}| < 1.5$, $\langle N_{\text{ch}} \rangle_{pA}$, were obtained as 8.1 ± 0.6 and 12.4 ± 2.1 at 400-GeV and 19-TeV proton collisions, respectively. Assuming that the coefficient of target nucleon effect in the central region is equal to $R_A = 1.61$,[19] the multiplicity in proton-nucleon collisions, $\langle N_{\text{ch}} \rangle_{pp}$, should be reduced to 5.0 ± 0.4 and 7.7 ± 1.4 for 400-GeV and 19-TeV collisions, respectively.

In Fig. 11(b), the angular distribution of γ rays is shown for 32 proton collisions with average energy of 8 ± 1 TeV, as well as the result at 400 GeV. In our experiment, γ rays with energy $E_\gamma > 30$ GeV and emission angle $\theta_\gamma < 10$ mrad can be detected. We note that the number of γ rays also increases with incident energy.

The angular distribution of charged secondaries produced in helium-lucite collisions with energy over 3.5 TeV per nucleon is shown in Fig. 12(a). The average multiplicity in $|\eta^{\text{c.m.}}| < 1.5$, $\langle N_{\text{ch}} \rangle_{\alpha A}$, is 24.3 ± 4.2 at incident energy 7 ± 2 TeV per nucleon. In Fig. 12(b), the angular distribution of γ rays is shown for 13 helium collisions with average incident energy of 7 ± 3 TeV per nucleon.

We can estimate the rate of missing γ rays with emission angle $\theta_\gamma < 10$ mrad from Figs. 11(b) and 12(b). If the multiplicity of neutral π mesons is half that of charged π mesons in this emission-angle region, the missing rate of γ rays is estimated to be 70% of the observed number. This value is used in making corrections for the invariant distributions of γ rays in the regions $P_{T\gamma} < 0.3$ GeV/c,

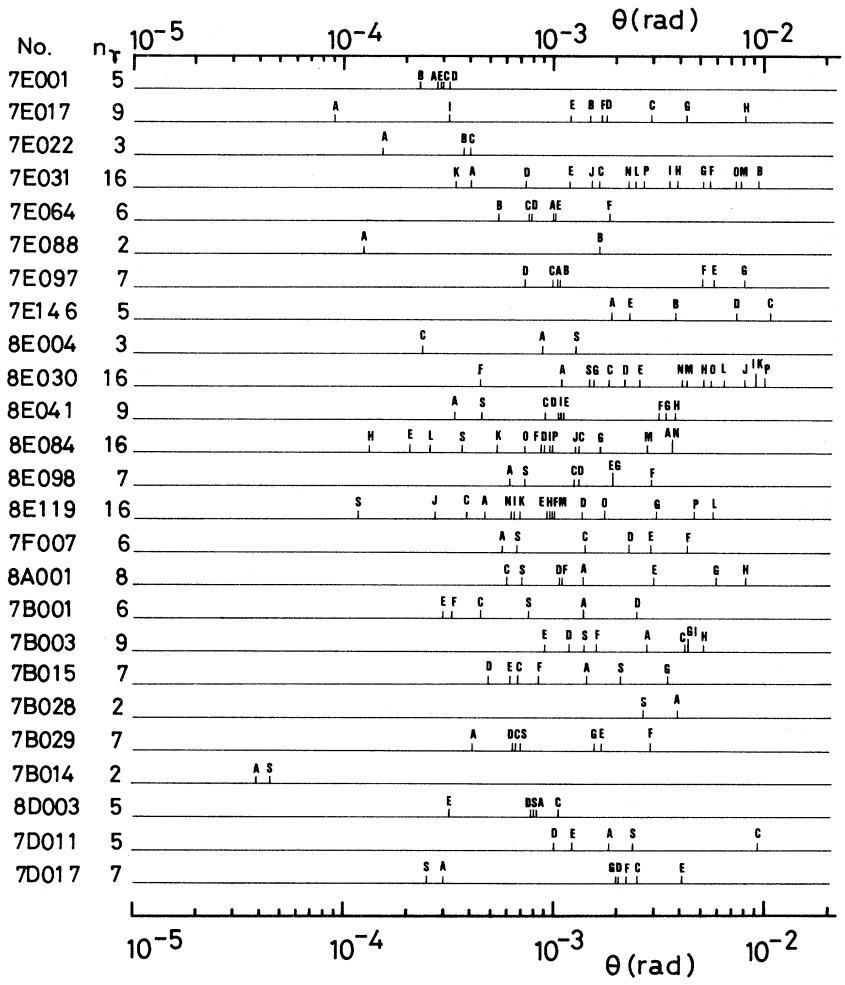

FIG. 10. Emission angles of γ rays relative to the estimated axis of the event.

$x_\gamma < 0.02$, and $f_\gamma < 0.05$, as described below.

E. Transverse-momentum distribution of γ rays and charged particles

In order to analyze the energy dependence of the γ-ray and charged-secondary-particle inclusive distribution, we use the invariant cross section, which is used in the accelerator experiments

$$F(x,P_T,s)=\frac{2E^*}{\pi\sqrt{s}}\frac{d^2\sigma}{dx\,dP_T{}^2} \tag{8}$$

with E^* being the energy of the particle in the center-of-mass system, s being the square of the total center-of-mass energy, x being the Feynman variable defined as $x=2P^*_{\parallel}/\sqrt{s}$, and $P^*_{\parallel}$ being the longitudinal momentum of the particle in the center-of-mass system.

The plot of $P_{T\gamma}$ against θ_γ is shown in Fig. 13. It is evident from this figure that the detection threshold energy is 30 GeV and this fact causes a detection bias against γ rays of low transverse momentum $P_{T\gamma}<0.3$ GeV/c.

We use the P_T distribution by integrating Eq. (8) over x,

$$\frac{1}{\sigma_{\text{inel}}}\frac{d\sigma}{dP_T{}^2}=\frac{1}{n}\frac{dN}{dP_T{}^2}\,, \tag{9}$$

where σ_{inel} is the inelastic cross section. The differential transverse-momentum distribution of γ rays in the forward hemisphere are shown in Fig. 14 for 32 proton collisions and 13 helium collisions. Our results for 303-GeV/c protons are also

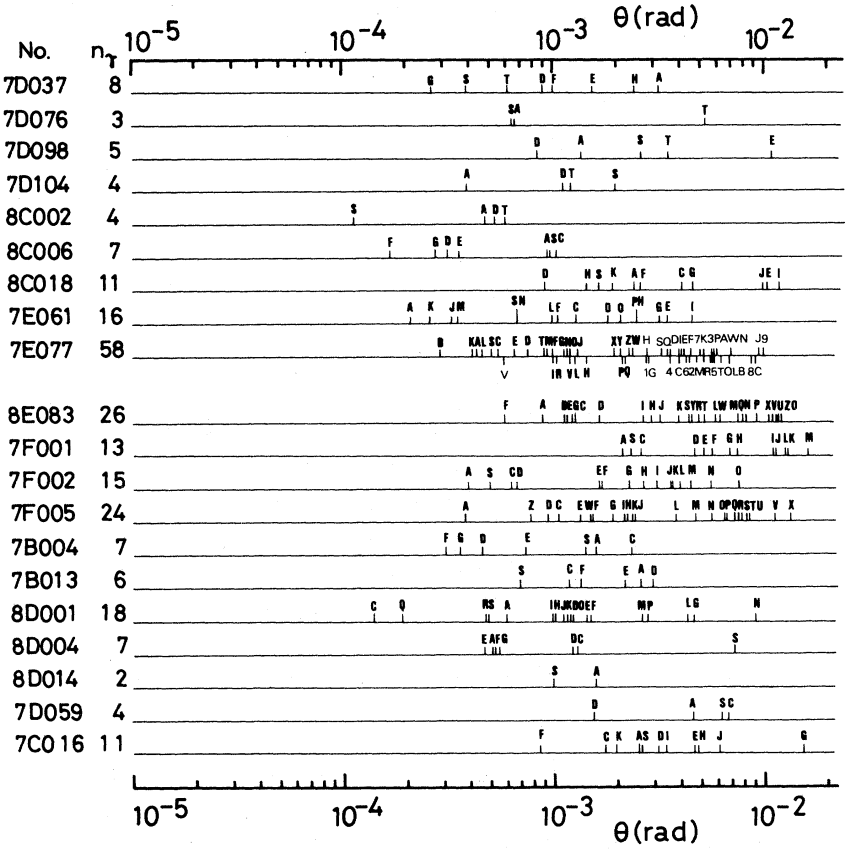

FIG. 10. (*Continued.*)

shown for comparison. In the range of $P_{T\gamma}<1.0$ GeV/c, average values of P_T and P_T^2 of γ rays were determined. The results are listed in Table III. By use of the formula

$$\langle P_T^2\rangle_{\pi^0}=3\langle P_T\rangle_\gamma^2-\tfrac{1}{2}M_{\pi^0}^2 \tag{10}$$

we are able to determine the average P_T^2 values for π^0 mesons assuming that all γ rays originated from π^0 decays.[20] One overestimates $\langle P_T\rangle_{\pi^0}$ by a few percent using $2\langle P_T\rangle_\gamma$.[21] We observe that $\langle P_T\rangle_\gamma$ does not change with incident energy from 303 GeV to 8 TeV. Our result at 303 GeV/c agrees

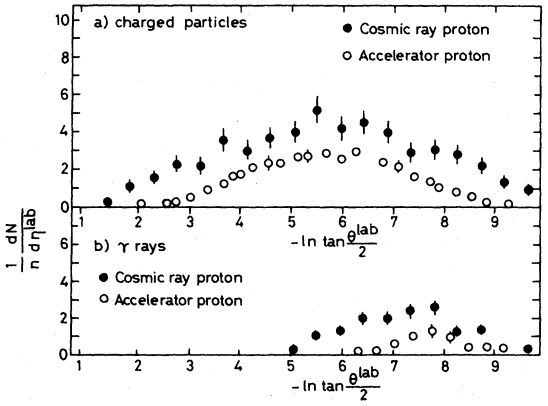

FIG. 11. Angular distribution of secondary (a) charged particles and (b) γ rays in cosmic-ray proton and 400-GeV accelerator proton collisions.

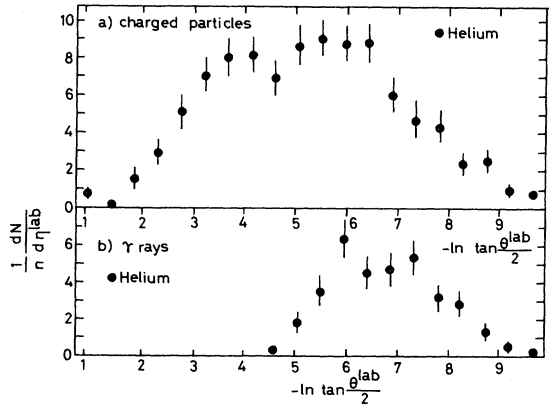

FIG. 12. Angular distribution of secondary (a) charged particles and (b) γ rays in helium collisions.

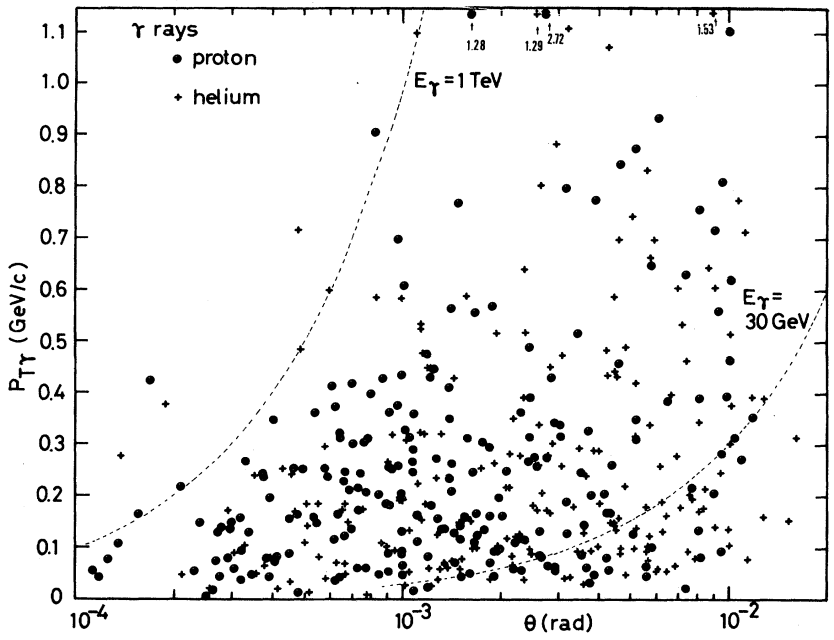

FIG. 13. Plot of transverse momentum of γ rays $P_{T\gamma}$ versus their emission angles θ_γ. The dashed lines correspond to $E_\gamma = 30$ and 1000 GeV.

well with the values obtained by Jaeger *et al.*[22] and Charlton *et al.*[21] at 200 GeV/c.

We can determine momenta of charged particles by measuring the multiple Coulomb scattering in the analyzer layers as described before. In the present analysis, however, this method has been applied only to a special event B07E31. To get the transverse-momentum distribution of charged particles, we quote here seven other cosmic-ray jet showers already analyzed by this method which were observed with the same type of emulsion chamber at airplane and balloon altitudes.[23] Table IV is the list of those events. The average value of incident energy was 11 ± 4 TeV. We also analyzed 70 events in a similar type of emulsion chamber exposed to 303-GeV/c proton beams.[10] Assuming the most energetic charged particle in the forward hemisphere to be the leading proton, we do not include this charged particle in the inclusive distribution. The $P_T{}^2$ distributions of charged particles in the forward hemisphere are shown in Fig. 15. The results of 205- and 12-GeV/c proton-proton collisions reported by Whitmore[24,25] are shown in the same figure. The increase in the inclusive differential cross section at cosmic-ray energies is a reflection of the increase in the charged multiplicity, since the area under the data points is proportional to the average number of charged particles produced. However, the shapes are different: At the higher energies the cross section is larger at region of $P_T{}^2 > 1.0$ (GeV/c)^2. The average values of P_T and $P_T{}^2$ are listed in Table III. The value of $\langle P_T \rangle$ for charged particles with $P_T < 1.0$ GeV/c is independent of incident energy from 100 GeV to 10 TeV. It should be kept in mind that most of the high-P_T particles are from the events AllC34 (Ref. 26) and B07E31 (Ref. 27) with the candidates of the X particles.

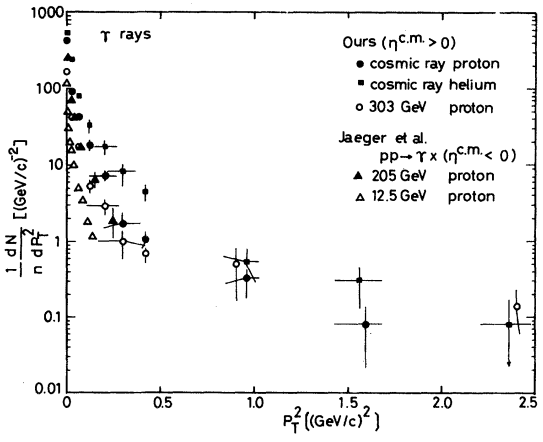

FIG. 14. Differential $P_T{}^2$ distributions of γ rays for cosmic-ray proton collisions at 8 TeV and helium collisions at 7 TeV per nucleon. Our result of 303-GeV proton collisions is shown in the same figure.

TABLE III. Average values of P_T and P_T^2 of γ ray, π^0 meson, and $\pi^{\pm}$ meson.

Incident Particle	$\langle P_T\rangle_\gamma$ (GeV/c)	$\langle P_T^2\rangle_\gamma$ [(GeV/c)^2]	$\langle P_T\rangle_{\pi^0}$ (GeV/c)	$\langle P_T^2\rangle_{\pi^0}$ [(GeV/c)^2]	$\langle P_T\rangle_{\pi^\pm}$ (GeV/c)	$\langle P_T^2\rangle_{\pi^\pm}$ [(GeV/c)^2]
303-GeV proton (ours)	0.196±0.011	0.067±0.004	0.392±0.022	0.192±0.012	0.333±0.022	0.151±0.010
10-TeV proton (ours)	0.200±0.010	0.071±0.004	0.400±0.020	0.203±0.012	0.350±0.037	0.189±0.020
7-TeV/nucleon helium (ours)	0.202±0.011	0.072±0.004	0.404±0.022	0.206±0.012		
200-GeV proton (Ferbel)					0.335±0.012	0.165±0.007
100-GeV proton (Ferbel)					0.341±0.020	0.172±0.020
200-GeV proton (Jaeger)	0.199±0.008	0.078±0.001	0.398±0.016	0.224±0.003		
12-GeV proton (Jaeger)	0.155±0.025		0.310±0.050			

F. Fractional-energy distribution of γ rays

The fractional energy of a γ ray is defined by $f_\gamma = E_\gamma / \sum E_\gamma$ and the differential distribution of f_γ for $f_\gamma > 0.02$ is shown in Fig. 16. In the region of $0.1 < f_\gamma < 0.7$, the spectra are represented by a single exponential of the form

$$\frac{1}{n}\frac{dN}{df_\gamma} = \text{const} \times \exp(-f_\gamma / f_0) , \tag{11}$$

where f_0 takes the value of 0.16 in proton collisions, and 0.15 in helium collisions. The results obtained by two other groups are also shown in the same figure[4,28] for comparison.

G. The x distributions of γ rays and charged particles

To analyze the energy dependence of x distribution, we define the function F_1 integrating Eq. (8)

TABLE IV. The list of events in which $\sum E_{ch}$ has been measured by the relative scattering method.

Event name	n_γ	n_s	$\sum E_\gamma$ (TeV)	$\sum E_{ch}$ (TeV)	E (TeV)
Neutral-lucite					
A11C34	35	70	8.38	10.74	31.87
Proton-lead					
A06D01	11	24	1.77	5.28	11.75
Proton-lucite					
B01-44	13	35	1.35	3.34	7.82
A04B57	13	21	1.55	1.74	5.48
A06C11	9	19	0.83	1.45	3.80
B03A11	9	17	1.18	0.84	3.37
AllB53	5	7	1.00	0.61	2.68
B07E31	16	58	1.29	11.92	22.02

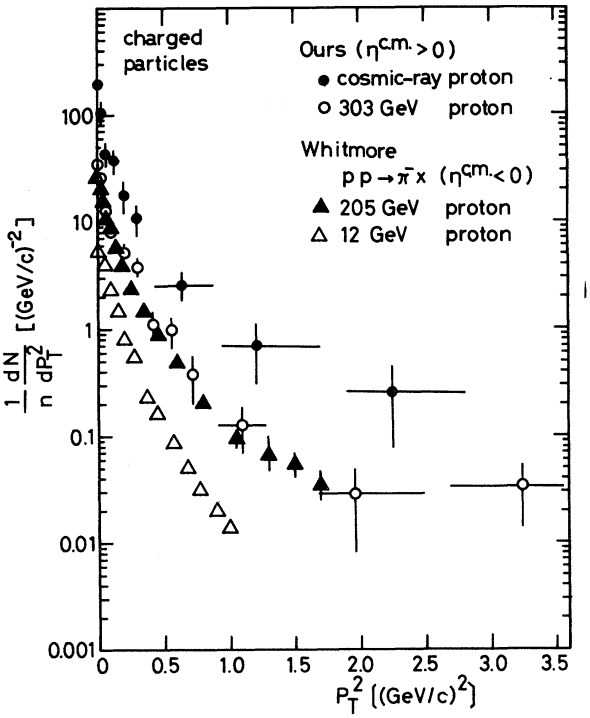

FIG. 15. Differential $P_T{}^2$ distributions of charged particles for cosmic-ray proton collisions at 11 TeV. Our result of 303-GeV proton collisions is also shown.

over $P_T{}^2$:

$$F_1(x,s)=\int \frac{2E^*}{\pi\sqrt{s}}\frac{d^2\sigma}{dx\,dP_T{}^2}dP_T{}^2 . \tag{12}$$

If the Feynman scaling law holds, this function

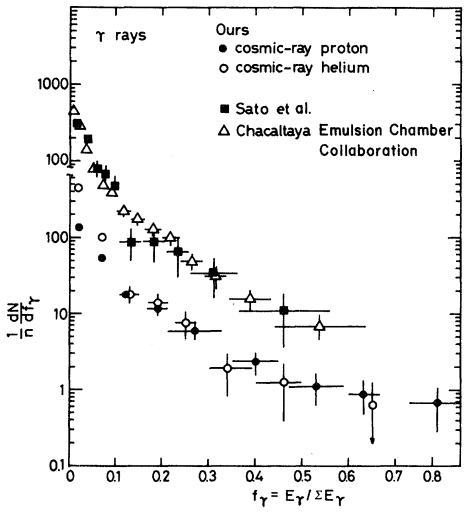

FIG. 16. Fractional-energy distributions of γ rays $f_\gamma=E_\gamma/\sum E_\gamma$, for cosmic-ray proton collisions and helium collisions.

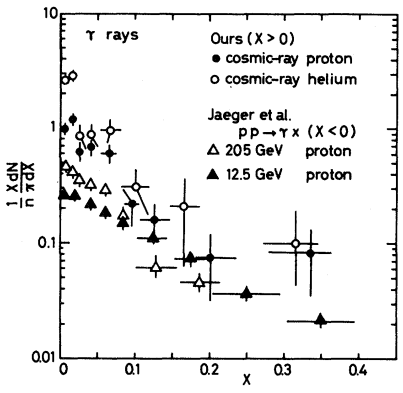

FIG. 17. The x distributions of γ rays for cosmic-ray proton collisions and helium collisions. The results of 12.5- and 205-GeV proton collisions reported by Jaeger *et al.* are shown.

should be independent of s. We have approximately the relation

$$F_1(x,s)/\sigma_{\text{inel}}=\frac{1}{n}\frac{x}{\pi}\frac{dN}{dx} \tag{13}$$

in the forward hemisphere. The x value is calculated by the relation

$$x=\frac{2P^*}{\sqrt{s}}=\frac{2P_T}{\sqrt{s}\tan\theta^*}$$
$$=\frac{E^{\text{lab}}}{2\gamma_c{}^2 M_P}[1-(\gamma_c\tan\theta^{\text{lab}})^2] , \tag{14}$$

where γ_c is the Lorentz factor of the c.m. system, which is estimated assuming the primary energy calculated by Eq. (5). The x distributions of γ rays are shown in Fig. 17 for proton collisions and heli-

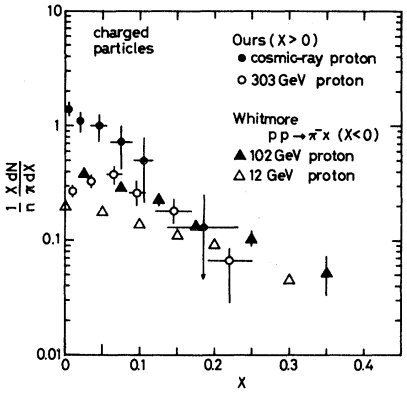

FIG. 18. The x distributions of charged particles for cosmic-ray proton collisions. Our result of 303-GeV proton, and the results of 12- and 102-GeV proton reported by J. Whitmore are shown.

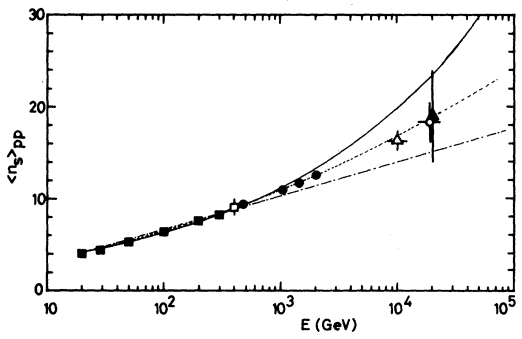

FIG. 19. Our cosmic-ray data (○) on average charged multiplicity are compared to the extrapolations of the accelerator data. Accelerator points (●) are from Thomé *et al.* The point (□) was obtained in an exposure to 400-GeV proton at Fermilab of the same type of emulsion chamber. The points (■) are from the other data of Fermilab. The point (△) is from Chaudhary and Malhotra, and point (▲) from Sato *et al.* The dashed curve represents $a+b(\ln s)+c(\ln s)^2$, the solid curve $a+s^{1/4}$, and the dot-dashed curve $a+b(\ln s)$.

um collisions. The x distributions of charged particles are shown in Fig. 18. The accelerator results reported by Jaeger *et al.*[22] and Whitmore[24] are also shown.

V. DISCUSSIONS

A. Multiplicity distribution

The corrected average multiplicity of secondary charged particles in proton-lucite collisions is obtained to be $\langle n_s \rangle_{pp}=18.3\pm2.2$ at 19 ± 4 TeV, and $\langle n_s \rangle_{pp}=9.0\pm0.8$ at 400 GeV/c. Cosmic-ray data on average charged multiplicity are compared with the extrapolations of the accelerator data. The energy dependence is shown in Fig. 19 together with the results of Fermilab and ISR experiments. The energy dependence of the form $\langle n_s \rangle_{pp}=a+b(\ln s)$ is excluded by our data. The present result can be fitted to the curve

$$\langle n_s \rangle_{pp}=a+b(\ln s)+c(\ln s)^2 , \tag{15}$$

where $a=0.88$, $b=0.44$, and $c=0.118$ as obtained by Thomé *et al.*[6] Sato *et al.*[4] estimated the average multiplicity to be 19 ± 5 in nucleon-nucleon collisions at about 20 TeV, which was obtained from 8 events with primary energy over 7 TeV. In the earlier emulsion-stack data, Chaudhary and Malhotra[29] selected 54 events with one or at most two heavy prongs, with primary energy in the range of 2—45 TeV (the mean energy was 10 ± 2 TeV). They estimated the average multiplicity to be 16.3 ± 1.1. The average multiplicity proportional to $s^{1/4}$ is a characteristic of thermodynamic models, and the logarithmic form is a characteristic of the conventional scaling picture. The above three results are well on the line extrapolated using Eq. (15). We conclude that the multiplicity is increasing more rapidly with energy than expected from the conventional scaling picture (i.e., increasing linearly with $\ln s$) toward 20 TeV.

The corrected average multiplicity is obtained to be $\langle n_s \rangle_{\alpha A}=49.3\pm7.8$ in helium-lucite collisions at 7 ± 2 TeV per nucleon. The ratio of the mean multiplicity in helium-lucite collisions to that in proton-lucite collisions at the same energy per nucleon can be obtained. The multiplicity for proton-proton collisions at 7 TeV is estimated to be 15.8 from Eq. (15), considering target effect. We get $\langle n_s \rangle_{pA}=23.8$ in proton-lucite collisions at 7 TeV. The ratio $R_{\rm ch}$ is estimated as

$$R_{\rm ch}=\langle n_s \rangle_{\alpha A}/\langle n_s \rangle_{pA} = 2.1\pm0.4 \text{ at 7 TeV} .$$

This value is to be compared with the theoretical one estimated by Eq. (6), which is $\langle \nu \rangle=2.0$ for $\langle A \rangle_{\rm lucite}=11$. Recently, preliminary results have been reported on α-α collisions with $\sqrt{s}=31.2$ GeV at ISR (R418).[7] The ratio of the mean multiplicity of negative charged particles in α-α collisions to that in p-p collisions at the same momentum per nucleon thus obtained is

$$R_{\rm neg}=\langle n_- \rangle_{\alpha\alpha}/\langle n_- \rangle_{pp}=1.6\pm0.1 .$$

The ratio $R_{\rm ch}$ from cosmic-ray data is larger than $R_{\rm neg}$ from ISR data. This may be reasonably understood, since the target nucleus is lucite in the cosmic-ray experiment.

B. Angular distribution

In order to investigate the details about the rise of the central particle density in proton collisions, we have analyzed the average charged-particle multiplicity in the pseudorapidity interval $|\eta^{\rm c.m.}|<1.5$. Both our results at 19 TeV and 400 GeV and other results at ISR energies obtained by Thomé[6] *et al.* are well fitted by a formula

$$\langle N_{\rm ch} \rangle_{pp}=a+b(\ln\sqrt{s}) , \tag{16}$$

where $a=-0.07$ and $b=1.48$. They are shown in

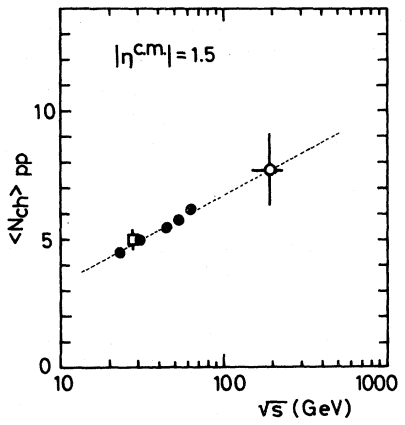

FIG. 20. Our cosmic-ray data (○) on mean charged-particle multiplicity in the interval $|\eta^{c.m.}|<1.5$ are compared to the extrapolations of the accelerator data. Accelerator points (●) are from Thomé *et al.* The point (□) was obtained in the exposure to 400-GeV proton at Fermilab. The dashed curve represents $a+b(\ln s)$.

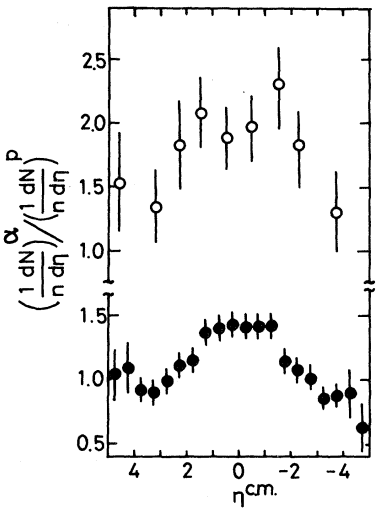

FIG. 21. The ratio (○) of rapidity densities for helium collisions at $\sqrt{s}=118$ GeV per nucleon to densities for proton collisions at $\sqrt{s}=200$ GeV from cosmic-ray data, and the ratio (●) densities for α-α at $\sqrt{s}=31.2$ GeV per nucleon to densities for p-p at $\sqrt{s}=62$ GeV from ISR data (CERN-Heidelberg-Lund Collaboration).

Fig. 20. This result gives the evidence for a substantial increase of particle density in the central plateau, and for violation of Feynman scaling in the central region within the energy range from ISR energies to 19 TeV. A significant part of the observed rise with energy of central rapidity density, however, may be a consequence of radial scaling.[30]

We have observed the higher density value of charged secondaries in the central region in helium-lucite collisions in Fig. 12. The ratio of rapidity density in helium-lucite collisions at $\sqrt{s}=118$ GeV per nucleon to that in proton-lucite at $\sqrt{s}=200$ GeV from cosmic-ray data is shown in Fig. 21. The ratio of α-α at $\sqrt{s}=31.2$ GeV per nucleon to proton-proton at $\sqrt{s}=62$ GeV from ISR data is shown in the same figure for comparison. The rapidity density ratio in the central region seems independent of $\eta^{c.m.}$. It is 2.0 in the rapidity region $|\eta^{c.m.}|<2.0$ for cosmic-ray data, and is 1.4 in $|\eta^{c.m.}|<1.5$ for ISR data. The rapidity density has the tendency to decrease with $\eta^{c.m.}$ in the region of $|\eta^{c.m.}|>2.0$. This tendency is seen in cosmic-ray events as well as in ISR. In this analysis, the remarkable feature is the significant increase of rapdidity density in the region of $|\eta^{c.m.}|<2.0$ in the cosmic-ray events.

C. Transverse-momentum distribution

Our results at 303-GeV/c accelerator proton collisions agree well with the data of γ rays obtained by Jaeger *et al.*[22] and Charlton *et al.*,[20] as well as the data of charged particles reported by Whitmore[24] and Ferbel.[25] The average values of P_T and P_T^2 in the region of $P_T<1.0$ GeV/c for γ rays and charged particles in proton collisions and helium collisions at both several hundred GeV/c and 10 TeV range show no difference within the experimental accuracy. However, at higher energy around 10 TeV the shapes of P_T distribution are different; the cross section for $P_T>1.0$ GeV/c becomes larger.

Sato *et al.*[4] and Agrawal *et al.*[5] reported a slow increase of the average P_T value of π^0 mesons with incident energies, but we did not observe an increase of $\langle P_T\rangle$ and $\langle P_T^2\rangle$ in the region of $P_T<1.0$ GeV/c for γ rays and charged particles. In our experiment we can detect the charged particles with no bias, and can measure the momentum by the method of relative scattering. In getting $\langle P_T\rangle$, we have considered the correction for low-energy γ rays. In our case, γ rays with the energy $E_\gamma<30$ GeV are not detectable. We used the same method for $\langle P_T\rangle$ determination in the accelerator experiments.

D. Fractional-energy distribution

The fractional-energy distributions of γ rays have been obtained by several groups.[2,4,5,28] Our

results on the fractional-energy distribution in the region of $f_\gamma > 0.1$ is in general agreement with these results. It is concluded that the fractional-energy distributions in this region is independent of incident energies. We observed the excess of γ-ray number in the region of $f_\gamma < 0.1$ in helium collisions in comparison with that in proton collisions. This corresponds to the excess of the ratio of the rapidity density of charged particles in the central region for helium collisions to that of proton collisions. The manner in which f_γ distribution in $f_\gamma < 0.1$ varies with different primary nucleus and incident energies presents an interesting problem.

E. The x distribution

The x distribution $F_1(x,s)$ in proton-proton collisions has been obtained by Jaeger *et al.*,[22] Charlton *et al.*,[21] Dao *et al.*[31] for γ rays, and by Whitmore[24] for charged particles, using hydrogen bubble chambers. The secondary particles detected in our experiment are those emitted in the forward hemisphere in proton and helium collisions. The target-nucleus effect is negligibly small. Our x distributions presented in Figs. 17 and 18 are steeper than those of the accelerator data in the region $x < 0.1$. This shows that the scaling of x distribution does not hold in the region of $x < 0.1$ at 10 TeV. This is consistent with the results from the angular distribution of charged particles, and suggests that the multiplicity of produced particles increase substantially in the central region at the energy from several hundred GeV up to 20 TeV. However, the scaling violation is small in the fragmentation region, $x > 0.1$.

Comparing the x distribution for helium collisions with that for proton collisions, it seems that the observed value $F_1(x,s)/\sigma_{\text{inel}}$ for helium collisions is approximately twice as large as that for proton collisions. This can be understood by supposing that on the average two nucleons of the helium projectile undergo inelastic collisions in traversing a lucite target nucleus. This agrees with the ratio $R_{\text{ch}} = 2.1$ and the value $\langle \nu \rangle = 2.0$ for helium-lucite collisions, the latter being calculated by Eq. (5).

VI. CONCLUSIONS

We have presented experimental results on inclusive γ-ray and charged-meson production in proton-lucite collisions at 20 TeV, and helium-lucite collisions at 7 TeV per nucleon. The main results are the following:

(1) The average charged multiplicity in proton-lucite collisions at 19 TeV is observed to be 25.2 ± 3.0. The corrected average charged multiplicity in p-p collisions, $\langle n_s \rangle_{pp} = 18.3 \pm 2.2$, agrees well with the value expected by the energy dependence of the form $\langle n_s \rangle_{pp} = 0.88 + 0.44(\ln s) + 0.118(\ln s)^2$ obtained by Thomé *et al.* at ISR energy range. The average charged multiplicity in helium-lucite collisions is observed to be 49.3 ± 7.8 at 7 TeV per nucleon. This value corresponds to 2.1 ± 0.4 times of that in proton-lucite collisions at the same energy.

(2) A substantial increase of charged secondaries in proton-lucite collisions is observed in the central region $|\eta^{\text{c.m.}}| < 1.5$ as the primary energy increases from several hundred GeV to 19 TeV. A linear rise of density in the form $\langle N_{\text{ch}} \rangle_{pp} = -0.07 + 1.48(\ln\sqrt{s})$ is observed, giving evidence for a violation of Feynman scaling at the energy around 20 TeV. The ratio of the rapidity density for helium-lucite at 7 TeV per nucleon to that for proton-lucite at 19 TeV is constant at 2.0 for the rapidity interval $|\eta^{\text{c.m.}}| < 2.0$.

(3) The transverse-momentum distributions of γ rays and charged π mesons are measured in the forward hemisphere of $\theta < 10^{-2}$ rad and $P_T < 2.0$ GeV/c. The average transverse momentum of γ rays for $P_T < 1.0$ GeV/c is 0.20 ± 0.1 GeV/c in proton-lucite collisions at 8 TeV and helium-lucite collisions at 7 TeV per nucleon, and that of charged π mesons for $P_T < 1.0$ GeV/c is 0.35 ± 0.04 GeV/c in proton-lucite collisions at 11 TeV. No difference of the average values of P_T and P_T^2 in $P_T < 1.0$ GeV/c is observed at both several hundred GeV/c and 10 TeV ranges. On the other hand, P_T distribution for $P_T > 1.0$ GeV/c at the energy region around 10 TeV is different from that at several hundred GeV/c. In the higher-energy region, the cross section for large P_T increases.

(4) The fractional-energy distribution of γ rays in the range $0.1 < f_\gamma < 0.7$ is represented by a single exponential,

$$dN/df_\gamma = const \times \exp(-f_\gamma/f_0) ,$$

where f_0 takes the value 0.16 in proton collisions and 0.15 in helium collisions. This is in agreement with the results obtained by several other groups. We observed the excess of γ-ray number in the region of $f_\gamma < 0.1$ in helium collisions in comparison

with proton collisions. This corresponds to the excess of the ratio of rapidity density of charged particles in helium collisions to that of proton collisions in the central region.

(5) The scaling of invariant distribution $F_1(x,s)$ for γ rays and charged π mesons in proton collisions in $x < 0.1$ does not hold at around 10 TeV, being consistent with an increase of particle density in the central region. However, the violation of scaling is small in the fragmentation region, $x > 0.1$. Comparing the x distribution in helium collisions with that in proton collisions, we have a picture that on the average two nuclei of helium projectile undergo inelastic collisions in traversing a lucite nucleus.

ACKNOWLEDGMENTS

The authors thank the Australia-Japan Foundation for providing financial assistance, and also the Institute for Space and Aeronautical Sciences, University of Tokyo, for technical and financial support. The Australian Balloon Station Team is thanked for carrying out these successful flights. Data analysis was made using the computer FACOM *M*-180 II of the Institute for Nuclear Study, University of Tokyo.

[1]O. Minakawa, Y. Maeda, Y. Tsuzuki, H. Yamanouchi, A. Aizu, H. Hasegawa, Y. Ishi, S. Tokunaga, Y. Fujimoto, S. Hasegawa, K. Niu, J. Nishimura, K. Nishikawa, K. Imaeda, and M. Kazuno, Nuovo Cimento Suppl. 11, 124 (1957).

[2]P. K. Malhotra, P. G. Chukla, S. A. Stephens, B. Vijayalakshmi, J. Boult, M. G. Bowler, P. H. Fowler, H. L. Hackforth, and J. Keereetaveep, Nuovo Cimento 49, 404 (1965).

[3]Y. Maeda, J. Phys. Soc. Jpn. 21, 1 (1966).

[4]Y. Sato, H. Sugimoto, and T. Saito, J. Phys. Soc. Jpn. 41, 1821 (1976); H. Sugimoto, Nuovo Cimento 53A, 82 (1979).

[5]A. K. Agrawal, R. Hasan, and M. S. Swami, Pramana 12, 45 (1979).

[6]W. Thomé, K. Eggert, K. Giboni, H. Lisken, P. Darriulat, P. Dittmann, M. Holder, K. T. McDonald, H. Albrecht, T. Modis, K. Tittel, H. Preissner, P. Allen, I. Derado, V. Eckardt, H. J. Gebauer, P. Meinke, P. Seyboth, and S. Uhlig, Nucl. Phys. B129, 365 (1977).

[7]*Discussion Meetings between Experimentalists and Theorists on ISR and Collider Physics,* Series 2, Number 2 (CERN, Geneva, 1981). This is a summary of the presentations of M. Valdata-Nappi (R210), T. J. M. Symons (R418), S. Frankel (R807), and R. Szwed (R418), 1981 (private communication). See also M. Jacob, in *Proceedings of the Fifth High Energy Heavy-Ion Study, Lawrence Berkeley Laboratory, 1981* (Lawrence Berkeley Laboratory, Berkeley, California, 1981), p. 581.

[8]H. Fuchi, K. Hoshino, S. Kuramata, K. Niu, K. Niwa, H. Shibuya, S. Tasaka, Y. Yanagisawa, Y. Maeda, and N. Ushida, in *Cosmic Rays and Particle Physics—1978,* proceedings of the Bartol Conference, edited by T. K. Gaisser (AIP, New York, 1979), p. 49.

[9]C. F. Powell, P. H. Fowler, and D. H. Perkins, *The Study of Elementary Particles by the Photographic Method* (Pergamon, London, 1959), p. 587.

[10]H. Fuchi, K. Hoshino, S. Kuramata, K. Niu, K. Niwa, S. Tasaka, Y. Yanagisawa, N. Ushida, and Y. Maeda, Nuovo Cimento 45A, 471 (1978).

[11]J. Nishimura, Prog. Theor. Phys. Suppl. 32, 72 (1964); J. Kidd and J. Nishimura, Nuovo Cimento Suppl. 1, 1086 (1963).

[12]N. Hotta, H. Munakata, M. Sakata, Y. Yamamoto, S. Dake, H. Ito, M. Miyanishi, K. Kasahara, T. Yuda, K. Mizutani, and I. Ohta, Phys. Rev. D 22, 1 (1980).

[13]K. Kasahara, S. Torii, and T. Yuda, in *Sixteenth International Cosmic Ray Conference, Kyoto, 1979, Conference Papers* (Institute for Cosmic Ray Research, University of Tokyo, Tokyo, 1979), Vol. 13, p. 70.

[14]H. H. Heckman, D. E. Greiner, P. J. Lindstrom, and H. Shew, Phys. Rev. C 17, 1735 (1978).

[15]M. J. Ryan, J. F. Ormes, and V. K. Balasubrahmanyan, Phys. Rev. Lett. 28, 985 (1972).

[16]F. Fumuro, R. Ihara, and T. Ogata, Nucl. Phys. B152, 376 (1979).

[17]P. L. Jain, M. Kazuno, Gerald Thomas, and B. Girard, Phys. Rev. Lett. 33, 660 (1974).

[18]E. Albini, P. Capiluppi, G. Giacomelli, and A. M. Rossi, Nuovo Cimento A32, 101 (1976).

[19]C. Halliwell, J. E. Elias, W. Busza, D. Luckey, L. Votta, and C. Young, Phys. Rev. Lett. 39, 1499 (1977).

[20]G. I. Kopylov, Phys. Lett. 41B, 371 (1972).

[21]G. Charlton, Y. Cho, M. Derrick, R. Engelmann, T. Fields, L. Hyman, K. Jaeger, U. Mehtani, B. Musgrave, Y. Oren, D. Rhines, P. Schreiner, H. Yuta, L. Voyvodic, R. Walker, J. Whitmore, H. B. Crawley, Z. Ming Ma, and R. G. Glasser, Phys. Rev. Lett. 29, 1759 (1972).

[22]K. Jaeger, D. Colley, L. Hyman, and J. Rest, Phys. Rev. D 11, 1756 (1975); 11, 2405 (1975).

[23]H. Fuchi, K. Hoshino, S. Kuramata, K. Niu, K. Niwa, S. Tasaka, Y. Yanagisawa, N. Ushida, Y. Maeda, and H. Kimura, in *Proceedings of the Fifteenth International Cosmic Ray Conference, Plovdiv, 1977,* edited by B. Betev (Institute for Nuclear Research and Nuclear Energy, Bulgarian Academy of Sciences,

Sofia, 1977), Vol. 7, p. 148.
[24]J. Whitmore, Phys. Rep. 10C, 273 (1974).
[25]T. Ferbel, in *Proceedings of the International Symposium on High Energy Physics at Tokyo, 1973* (Institute for Nuclear Study, University of Tokyo, Tokyo, 1973), p. 1.
[26]S. Kuramata, K. Niu, K. Niwa, K. Hoshino, E. Mikumo, Y. Maeda, T. Nagai, and S. Tasaka, in *Proceedings of the Thirteenth International Cosmic Ray Conference, Denver, 1973,* Conference Paper (University of Denver, Denver, Colorado, 1973), Vol. 3, p. 2239.
[27]H. Fuchi, K. Hoshino, S. Kuramata, K. Niu, K. Niwa, H. Shibuya, Y. Yanagisawa, S. Tasaka, V. D. Hopper, Y. Maeda, H. Kimura, Y. K. Lim, and N. Ushida, in *Sixteenth International Cosmic Ray Conference, Kyoto, 1979, Conference Papers* (Ref. 13), Vol. 6, pp. 112, 245.
[28]J. Bellandi Filho *et al.*, Brazil-Japan Emulsion Chamber Collaboration, in *Cosmic Rays and Particle Physics—1978* (Ref. 8), p. 94.
[29]B. S. Chaudhary and P. K. Malhotra, Nucl. Phys. B86, 360 (1975).
[30]R. W. Ellsworth, in *Sixteenth International Cosmic Ray Conference, Kyoto, 1979, Conference Papers* (Ref. 13), Vol. 7, p.333.
[31]F. T. Dao, D. Gordon, J. Lach, E. Malamud, J. Schivell, T. Meyer, R. Poster, P. E. Schlein, and W. E. Slater, Phys. Rev. Lett. 30, 1151 (1973).